IOP Conf. Series: Materials Science and Engineering **406** (2018) 012020 doi:10.1088/1757-899X/406/1/012020

Compaction behaviour of tow at meso-scale: experimental investigations of morphological evolution at dry, lubricated and saturated states

J Hemmer[1, 2*], A Sakkalatty Dharmalingam[1], A-S Lectez[1, 3], C Burtin[1], S Comas-Cardona[1], C Binetruy[1], T Savart[2]

[1]Institut de Recherche en Génie Civil et Mécanique (GeM) – Ecole Centrale de Nantes
[2]Plateforme CANOE
[3]Centre National d'Études Spatiales (CNES)

*julie.hemmer@ec-nantes.fr

Abstract. Tows, partially constrained (tows within textile architecture) or free (single tows) exhibit movements and deformations, due to the various mechanical solicitations applied during manufacturing. During weaving or stitching, single dry tows undergo local compaction due to interlacing or stitch, leading to the evolution of the tows cross-section while processing. Once the woven or non-crimp fabrics are produced, they are impregnated by a fluid: when considering the infusion process, the filling step leads to a global compressive unloading at macro-scale that modifies, in a saturated state, tows cross-section and tows spatial distribution within the fabric. These evolutions of the fibrous microstructure at mesoscopic scale impact both the mechanical properties and the permeability. Thus, this work proposes two novel experimental methodologies to quantify the morphological evolution of tows under compaction at dry, lubricated and saturated states.

1. Introduction

During textile fabrics and composites manufacturing, tows, partially constrained (tows within textile architecture) or free (single tows) exhibit movements and deformations, due to mechanical solicitations as compaction. Depending on the considered process, tows can either be in dry, lubricated or saturated states. For instance, during weaving or stitching, single dry tows undergo local compaction due to interlacing or stitch, leading to the evolution of the tows cross-section while processing. Several researchers have proposed different fabrics' mechanical modeling at various scales as presented and mentioned in, for example, the review articles [1, 2, 3]. However, very few authors measured and provided available data of the width and thickness evolution of tow under compression perpendicular to the fibers (as presented in [4]).

Woven or non-crimp fabrics are then impregnated by a fluid: when large composite parts (as wind blade turbine for instance) are considered, the infusion process is competitive on both mechanical and cost aspects. It is a closed mold composite process, where the bottom side of the mold is solid, and the top side is a vacuum bag. Because the vacuum bag is flexible, local compaction state of the porous fabric preform can easily be modified. In the saturated area of the part, far behind the flow front, a thickness rise of the fabrics is experimentally observed, due to the gradient of the resin pressure field [5, 6, 7]. The transient macroscopic thickness rise has been extensively studied but no microscopic evolution of the channels (meso-pores) and tows of a given sample has been proposed. However, the impact of the meso-

pores distribution, size and location on the global in-plane permeability of fabric is well-known [8, 9]: the global fiber volume fraction seems not fine enough to represent the flow paths and velocity inside a dual-scale fabric.

This work proposes two novel experimental methodologies to quantify the morphological evolution of constrained and free tows under compaction at dry, lubricated and saturated states. On one side, the cross-sectional dimensions (thickness and width) of single tows are measured under compaction using a chromatic confocal scanner. This method allows defining a normalized bounding box cross-section (NCS) for tows, whose evolution with compaction differs depending on the experimental conditions (dry or lubricated state, free tow). On the other side, a set-up is developed to realize in situ downsized infusion inside an X-ray Computed Tomography (XCT) device. 3D images of the same stack are recorded under dry and saturated states, for a quasi-unidirectional non-crimp fabric (quasi-UD NCF). Due to the fluid pressure rise between these two states, the fibrous stack is submitted to an unloading compressive phenomenon. The image processing of the associated microstructures allows quantifying the influence of the compaction state on tows morphological evolution.

2. Characterization of single tow evolution at dry and lubricated states

The method and results presented in this section have been recently published in [4]. First, a method for measuring and comparing tows (or yarns) geometrical evolution during compaction perpendicular to the fibers is presented. Then, results about the compacity evolution are extracted for a wide range of compaction levels.

2.1. Materials of the study

Two E-glass fiber tows (1200 and 4800 tex), and two high strength (HS) carbon fiber tows (6k and 12k) have been tested. The fibers are continuous filaments. Their specifications and features are given in table 1. The initial cross sections, considered as rectangular bounding boxes ($CS = w_0 h_0$ where w_0 is the initial width, and h_0 the initial thickness) are measured under a 2N compression force applied on the tow. Those 4 references have been chosen because they are constituted of 2 natures of fibers and they have different initial cross-section aspect ratios (AR) ranging from 3.1 to 12.2. The fibrous materials are tested in dry and lubricated states. For the lubricated states, the fiber tows are sprayed (below 5% in mass) with a lubricant constituted of aliphatic hydrocarbons and mineral oils (WD- 40 Company).

Table 1. Specifications of the materials of the study [4].

Material	Fiber nature	Tow features		
		Number of fibers per tow	Tow lineal weight (g/m)	Tow initial aspect ratio (w_0/h_0)
Glass 4800 tex	E-glass	8000	4.8	3.1
Glass 1200 tex	E-glass	2000	1.2	12.2
Carbon 12k	HS carbon	12000	0.90	5.0
Carbon 6k	HS carbon	6000	0.42	6.4

2.2. Methods

A compression device has been specially designed to apply uniaxial (z-direction) transverse compression on a sample tow under a chromatic confocal scanner (CCS Prima, STIL). This device is presented in figure 1. It is composed of a micrometric compact lab jack (LJ 750, Thorlabs), through which vertical displacements are applied, a 2 kN force cell (Type U3, HBM), a bottom polished steel plate on which lie the sample, and a top PMMA plate, bonded to a steel frame (two columns). Compaction forces from 2 to 150 N are consecutively applied on the samples in the z-direction. Each measurement is realized on the deformed sample few minutes after applying the force. The scan is

performed as shown in figure 2 at five different locations for each tow sample. Scanning the sample in the lateral direction (y-direction) provides its width as well as its thickness (figure 3). Three to five tow samples (5 cm long) are used for each tow reference. As the compaction force is increased on the free-edge (laterally unconstrained) tow, its thickness (z-direction, h) reduces and its width (y-direction, w) increases.

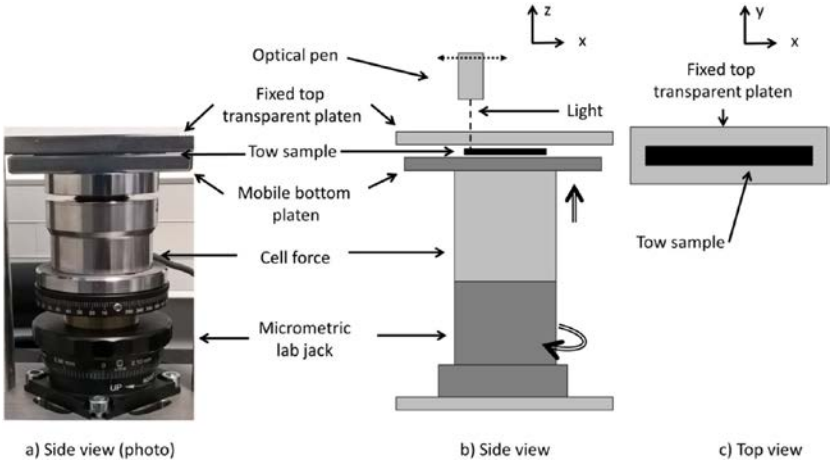

Figure 1. Compression set-up under chromatic confocal scanner [4].

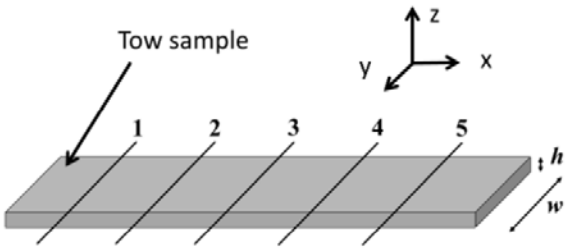

Figure 2. View of the tow sample and the 5 locations of the profiles [4].

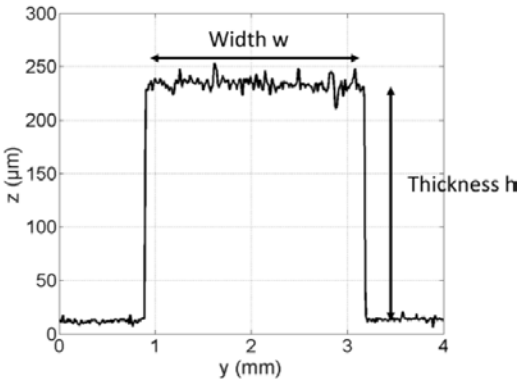

Figure 3. Example of a measured profile at a given location on the tow [4].

2.3. Results

Normalized bounding box cross-section (NCS) wh/w_0h_0 are measured and displayed. The thickness extension $\lambda_h = h/h_0$ is defined for sake of clarity. Fibrous (porous) tows exhibit some degree of compressible behavior as they are compacted. For instance, figure 4 illustrates the expected evolution of the NCS with respect to extension for various transverse (z-direction) compressibility behaviors of the tows. For highly compressible tows under uniaxial compaction, its width may not evolve, while the thickness will reduce and the material will densify (higher fiber volume fraction). For "incompressible" tows, as it is compacted in the thickness direction, the tow will flatten. The width will increase so as to maintain constant density (or constant fiber volume fraction). Some tows will behave in between those both extreme behaviors.

2.3.1. Dry state evolution. The results of the 4 tested references in a dry state are displayed in figure 5. The initially flattest tows (Carbon 6k and Glass 1200tex of aspect ratio 6.4 and 12.2 respectively) are experiencing a strong reduction of volume with limited lateral expansion as they are compacted. The flatter the tow initially, the less lateral expansion occurs as it is compacted. Those tows are densifying with compaction whereas the Glass 4800tex exhibits a flattening behavior.

2.3.2. Dry and saturated state evolution. The results of the 2 tested references in a lubricated state are displayed in figure 6. The results of the measurement are compared to the results obtained in the dry state. For both references the NCS is increasing when the tows are lubricated. The relative increase is more pronounced for the Glass 1200tex than for the Carbon 6k. For the flattest tow (Glass 1200tex), the lubrication allows for an enhanced flattening that could be due to the reduction of fiber/fiber friction.

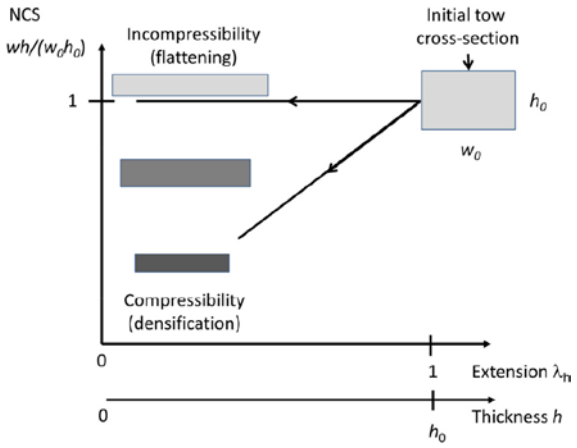

Figure 4. Evolution of the normalized bounding box cross-section (NCS) of the tows with respect to the extension or thickness for various compressibility behaviors [4].

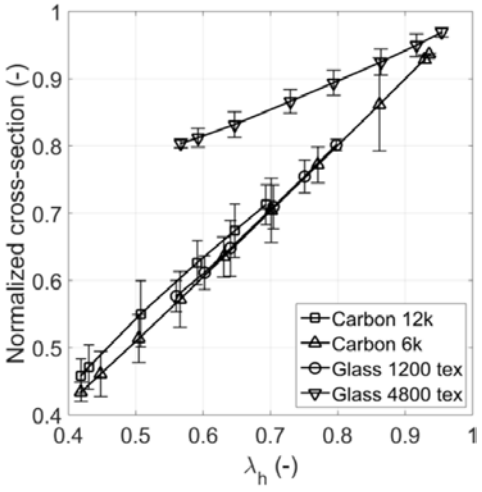

Figure 5. Normalized cross-section (NCS) with respect to extension for all tested dry tows [4].

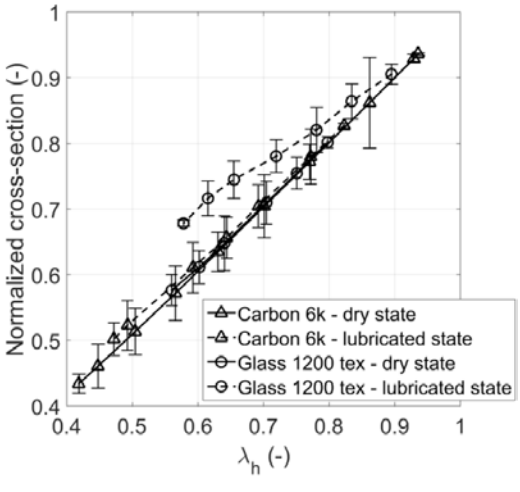

Figure 6. Normalized cross-section (NCS) with respect to z-extension for Carbon 6k and Glass 1200 tex in dry and lubricated states [4].

2.3.3. Conclusion. These methodology and analysis allow to follow free (not constrained in a fabric architecture) tows behavior for a wide range of compaction levels at dry and lubricated states. The four

different tested tows showed various behaviors at dry state. The Glass 4800tex exhibits a flattening behavior, its tow initial aspect ratio being low (3.1) whereas the initially flattest tows (Carbon 6k and Glass 1200tex of aspect ratio 6.4 and 12.2 respectively) are experiencing a limited lateral expansion as they are compacted.

3. Characterization of tow evolution inside a fabric between dry and saturated states

The method and results presented in this section have been submitted in [10]. First, a method to realize and post-process an *in situ* downsized infusion inside a XCT device is presented and results about tow deformation between the dry and the saturated states (unloading compressive phenomenon) are detailed.

3.1. Material

The quasi-unidirectional non-crimp fabrics (quasi-UD NCF) selected for the study are manufactured from batches of Advantex® glass roving (Owens Corning). A single ply is made of two layers: one warp layer of UD glass tows (4800 tex, presented in the table 1) and one weft backing glass layer oriented at 80° (68 tex). Both layers are stitched (warp-knitting) with a very thin polyester yarn, symmetrical and spaced of 5 mm that constrains locally the 4800 tex tows in width direction.

To impregnate the fibrous reinforcement, technical glycerol from VWR is used in dilution with 5% of distilled water (viscosity of 0.3 Pa.s at 25°C).

3.2. Methods

XCT experiments are conducted to record a given dual-scale fibrous microstructure evolution under several compaction states: one a dry state, and another one at saturated state. The adapted setup to realize downsized infusion process is described in [10]. The experimental methodology to record representative 3D images is detailed below and the post-processing methods used to analyse them are also presented.

3.2.1. Experimental procedure. A controlled level of vacuum (60 mbar abs) is applied in a cavity (hermetically closed with a vacuum bag) where plies of quasi-UD NCF are previously laid down (figure 7a), fiber direction being along the X-axis. It has been established that one hour of relaxation is necessary to stabilize the dry fabric. After this relaxation time, two 3D images are recorded with a XCT device: the first one near the fluid inlet (in red in figure 7b) and the second one near the vacuum vent (in orange in figure 7b). The microstructure M obtained near the inlet at dry state is illustrated in figure 7b.

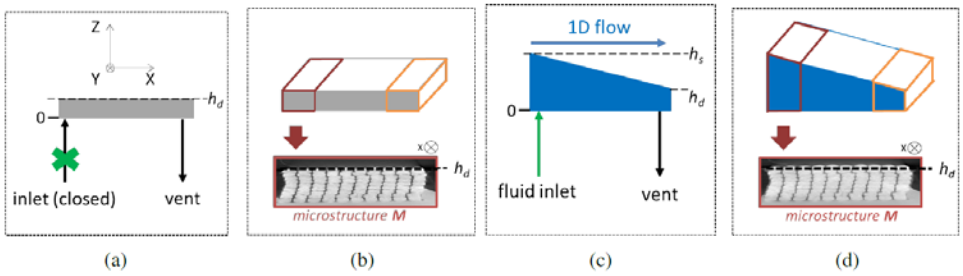

Figure 7. Experimental steps: (a) dry state. (b) dry state, XCT acquisition. (c) saturated state. (d) saturated state, XCT acquisition [10].

The filling step of the infusion process is launched: a 1D continuous flow of glycerol along the X-axis is maintained in the cavity, leading to a higher thickness near the fluid inlet when fully saturation is attained (figure 7c). Again, one hour of relaxation is needed for the saturated fabric stabilization. The same quasi-UD NCF sample is then under a flow-induced compaction state. Two 3D images are recorded at the locations chosen for the dry state acquisitions. The microstructure M at saturated state is illustrated in figure 7d.

3.2.2. XCT parameters. A XCT device (Micro-XCT400, Xradia company) with the objective Macro70 records and reconstructs the 3D images of the fibrous microstructure. The set of parameters (detailed in table 2) have been chosen to obtain the best ratio between a large enough region-of-interest (ROI) and sufficient resolution to determine a refined tow evolution. To ease the post treatment, the set of parameters is kept equal between the dry and the saturated states.

Table 2. Set of parameters for XCT acquisition [10].

	Value
Input parameters	
Number of images (-)	1947
Exposition time	20
Output parameters	
ROI (mm x mm x mm)	19 x 19 x 19
Resolution (µm/pixel)	10.6
Acquisition duration (h)	12

3.2.3. Image processing. Once the desired dry or saturated compaction state is reached in the XCT, image processing is used to detect the tow deformation. When reconstructed, the 3D image is a matrix Im(i,j,k), where i ∈ [1,m], j ∈ [1,n], and k ∈ [1,N]. A slice k is then an (m x n) image in the YZ-plane, and the 3D image is composed of N slices. Each value of the matrix, between 0 and 255, is a voxel gray-level value. Each k value corresponds to an X-location (a slice) in the fibrous reinforcement: X being the dimensionless position in the X-direction, X=0 is near the fluid inlet and X=1 is near the vacuum vent.

At a defined X-location (a slice YZ-plane), existing edge detection algorithms (for instance Canny or Sobel, as review in [11]) are not efficient to find the warp tows boundaries (figure 8c). This is mainly due to the weft backing glass layer of the fabrics, whose out-of-interest weft tows gray-levels are close to the warp tows gray-levels. Because the weft tows orientation is 80°, the horizontal channel in between two warp tows is easy to identify when moving toward the X-direction of a 3D image: an horizontal channel not detectable at a defined position X is visible at X+δX (figures 8a and 8b). A new image, considered as the concatenation of 100 slices (δx=100mm) around the slice k is then defined to get rid of the weft tows (figure 8d):

$$GLc_k(p) = \min_{k'=k-50 \rightarrow k+50} GL_{k'}(p) \quad (1)$$

where GLc_k is the gray-level concatened image around the centered slice k (k-50 to k+50), p is the considered pixel, $GL_{k'}$ is the gray-level slice k'. Applying an edge detection to these concatened images enhance drastically the detection of tows boundaries, as illustrated in figure 8.

At a given X-location, each tow area is computed at dry ($A_{dry}(X, tow)$) and saturated ($A_{saturated}(X, tow)$) states and the swelling of particular tow ($\alpha(X, tow)$) is defined as its area evolution between these two states:

$$\alpha(X, tow) = \frac{A_{saturated}(X,tow) - A_{dry}(X,tow)}{A_{dry}(X,tow)} \quad (2)$$

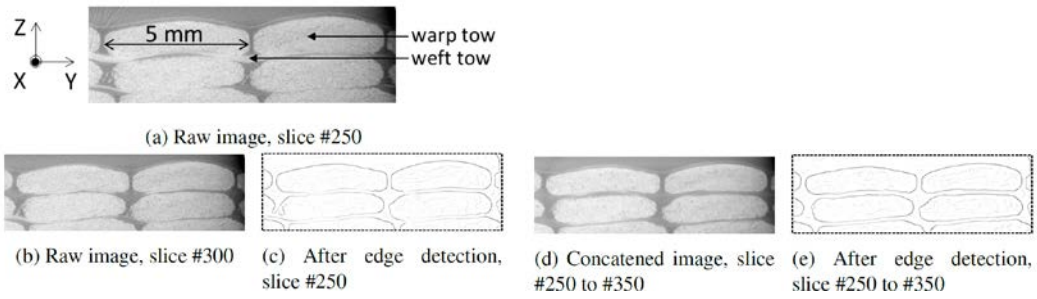

Figure 8. Illustration of image concatenation process and of its impact on tow detection enhancement [10].

3.3. Results

The results below are presented at a specific X-location (X=0.04), for a same fibrous microstructure recorded at dry and saturated states. Near the fluid inlet (X=0.04), the compressive unloading phenomenon induces the larger deformation along the stack thickness. Further analyses are detailed in [10].

3.3.1. Tow deformation. To enhance the visibility of each tow evolution, the centroids of dry tow and its corresponding saturated tow are superposed (figure 9c). Besides, the initial dry tow is represented in green, the final saturated tow is in pink, and the intersection between both is in white.

The tows area evolution ($\alpha(X, tow)$ *in %*) is not depending on the tow location inside the stack: tows near the vacuum bag and tows near the PVC plate evolve equally (figure 9c). The tow deformation occurs in the thickness direction (Z-axis); lateral tow deformation (Y-axis) is negligible. It could be explained by the stitch yarn (not visible in the recorded XCT images), whose limiting the spreading of tows during the compressive loading.

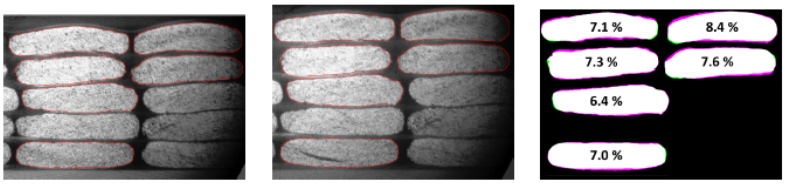

(a) X=0.04, dry, 60 *mbar* (b) X=0.04, saturated, 60 *mbar* (c) X=0.04, tows

Figure 9. Visualization of tows evolution between the dry and the saturated states. Percentages correspond to the values of α (X, tow) [10].

3.3.2. Conclusion. The proposed methodology and analysis allow following the behaviour of E-glass tows (4800 tex) inside a quasi-UD NCF, between the dry and the saturated states. Due to the fluid pressure rise between these two states, the fibrous stack is submitted to an unloading compressive phenomenon. Inside the stack, tows are undergoing large deformation: the area of tow can increase by 8%. Because the tows are partially constrained by the stitch yarn of the fabric, tow deformation occurs in the thickness direction (Z-axis) and lateral tow deformation (Y-axis) is negligible.

4. Conclusions and outlook

This study proposed two experimental setups to follow the tow behaviors under several boundaries conditions.

Using a chromatic confocal scanner, the behaviour of free tows has been characterized at both dry and lubricated states, for a wide range of compaction, perpendicular to fibers. The results show that for

initial flatness tows (high cross-section aspect ratio), a densification is observed as the compressive load is increasing. For initial more circular tows (4800 tex, with low cross-section aspect ratio), a flattening is observed as the compressive load is increasing. Also, for the flattest tow, the lubrication tends to enhance the tow flattening that could be due to the reduction of fiber/fiber friction.

Using an XCT device, the behaviour of partially constrained tow (tow inside a specific fabric architecture, referred as 4800 tex) has been followed from the dry to the saturated states. The tows located near the fluid inlet of the infusion setup undergo the highest level of compressive unloading, due to the fluid pressure rise. The results shows that tows are undergoing large deformation: the tow area can increase by 8%. This tow deformation occurs only in the thickness direction (Z-axis) because the stitch yarn is partially constraining the tow in the width direction (Y-axis).

These results illustrate that the tows behaviours under loading or unloading compression perpendicular to fibers seem to depend on several parameters: the initial aspect ratio of the tow, the lubrication state (dry, lubricated or saturated), and the spatial constrains (single tow or tow in a fabric).

Ongoing work is focused on the homogenization of the results presented in this study. The confocal chromatic setup is being modified to able dry, lubricated and saturated experiments, where wide range of loading and unloading compaction will be applied to free and constrained tows.

Acknowledgments
The authors would like to thank CANOE for their financial support so as the funding provided by the French ANRT by grants under CIFRE funding program. Jean-Michel Lebrun is gratefully acknowledged for its help to design setups.

References

[1] Boisse P, Colmars J, Hamila N, Naouar N and Steer Q 2018 *Compos B Eng* **141** 234-49
[2] Gereke T, Döbrich O, Hübner M, Cherif C 2013 *Compos Appl Sci Manuf* **46** 1–10
[3] Syerko E, Comas-Cardona S, Binetruy C 2012 *Compos Appl Sci Manuf* **43** 1365–88
[4] Dharmalingam A S, Hemmer J, Lectez A-S, Binetruy C, Comas-Cardona S 2018 *Composites Part B* **148** 235-42
[5] Tackitt K D, Walsh S M 2005 *Materials and Manufacturing Processes* **20** 607–627
[6] Yenilmez B, Senan M, Sozer E M 2009 *Composites Science and Technology* **69**
[7] Yang J, Xiao J, Zeng J, Jiang D, Peng C 2012 *Applied Composite Materials* **19** 443–58
[8] Salvatori D, Caglar B, Teixido H, Michaud V 2018 *Composites Part A* **108** 41–52
[9] Caglar B, Orgéas L, Rolland du Roscoat S, Sozer E M, Michaud V 2017 *Composites Part A* **99** 1–14
[10] Hemmer J, Burtin C, Comas-Cardona S, Binetruy C, Savart T, Babeau A 2018 *submitted in Composites Part A*
[11] Pal N R 1993 *Pattern recognition* **26** 1277–94